Hysteretic Beam Model for Steel Wire Ropes Hysteresis Identification

Biagio Carboni, Carlo Mancini and Walter Lacarbonara

Abstract A nonlinear hysteretic beam model based on a geometrically exact planar beam theory combined with a continuum extension of the Bouc-Wen model of hysteresis is proposed to describe the memory-dependent dissipative response of short wire ropes which have the unique feature of exhibiting hysteretic energy dissipation due to the interwire friction. With the proposed model, hysteresis is introduced in the constitutive equation between the bending moment and the curvature within the special Cosserat theory of shearable beams. The model is indeed capable of describing the hysteretic behavior exhibited by short steel wire ropes subject to flexural cycles. The model parameters which best fit a series of experimental measurements for selected wire ropes are identified employing the Particle Swarm Optimization method. The identified parameters are used to reproduce other experimental tests on the same wire ropes obtaining a good accuracy.

1 Introduction

Wire ropes are structural elements usually employed to resist large axial loads while providing high strength, durability and reliability. In these applications the ropes length is much larger than the diameter usually resulting in a negligible bending stiffness along the cable length except in regions near the boundaries or point loads where boundary layers are produced. On the contrary, when the wire ropes are relatively short (i.e., the ratio between length and diameter is comparable to that characteristic for beams) and subject to cyclic loadings, the bending stiffness cannot be neglected and the force-displacement response shows hysteresis loops due to the

B. Carboni · C. Mancini · W. Lacarbonara (✉)
Department of Structural and Geotechnical Engineering, Sapienza University of Rome,
Via Eudossiana 18, 00184 Rome, Italy
e-mail: walter.lacarbonara@uniroma1.it

B. Carboni
e-mail: biagio.carboni@uniroma1.it

C. Mancini
e-mail: mancinicarlo@libero.it

relative sliding between the wires. The idea of exploiting the bending behavior of short wire ropes to absorb and dissipate energy was proposed for the first time by Stockbridge in the last century [36]. More recently, several applications based on the interwire friction exhibited by short wire ropes have been explored [6, 11, 17, 18, 37, 43]. Within this context, Carboni et al. proposed a new rheological device capable of providing several types of hysteretic responses employing assemblies of wire ropes made of steel and shape memory alloy materials [5].

Challenging issues are inherent in the mathematical modeling and prediction of the complicated mechanical behavior of wire ropes. Costello [9] proposed a theory in which the individual wires are modeled using Loves equations for bending and twisting of thin helical rods [26]. However, this model does not describe the frictional effects. A direct approach based on the finite element method (FEM) consists in constructing solid models which, upon reflecting the actual helical wire rope geometry, are treated as a deformable continuum with frictional contacts [27, 30, 44]. The high computational burden due to the complexity associated with handling the evolving contact regions between the wires does not allow to use three-dimensional FEM models for predicting the wire rope hysteretic behavior. Analytical [20, 21] or semi-analytical methods based on one-dimensional polar continuum formulations supplemented by rheological models for the constitutive laws are more suitable for describing the hysteresis exhibited by wire ropes. Sauter and Hagedorn [32] extended the Masing model for a continuous system to model the short cables of a Stockbridge damper. Rafik and Gerges [16] developed a model based on a curved beam to describe wire rope springs deforming in tension-compression cycles.

A phenomenological model often used to describe the mechanical behavior of hysteretic systems is the Bouc-Wen (BW) model [3, 45]. It has been used in a wide variety of studies for modeling discrete hysteretic restoring forces or stresses. Several extended versions of the BW model have been proposed to take into account stiffness and strength degradation or pinching behavior [1, 2, 5]. Recently, the BW model has been generalized to continuous systems for describing materially nonlinear problems such as elastoplastic structures. Sivaselvan and Reinhorn [35], starting from the original model proposed by Bouc [3], developed a smooth hysteretic method based on the viscoplasticity theory in the context of the flexibility approach to simulate inelastic frame structures according to a state space formulation [34]. A three-dimensional BW-type model obtained by smoothening a three-dimensional yield surface was proposed by Casciati [7]. Triantafyllou and Koumousis [39] introduced an elastoplastic hysteretic constitutive relationship derived by the BW model in the classical Euler-Bernoulli beam formulation to conduct small and large displacement dynamic analysis of frame structures. The same authors [38, 40] extended the plastic formulation based on the BW model to plane stress elements.

Another important task in the design of applications that rely on hysteretic behaviors is represented by the identification of the model parameters on the basis of experimental measurements. Identification strategies can be classified according to several

criteria. A useful distinction is between parametric and non parametric methods. An example of a non parametric method is the restoring force method initially developed by Masri and Caughey [28] and by Donnell and Crawley [10]. This method deals with the identification of nonlinear dynamical systems for which accelerations, velocities and displacements are directly measured or obtained via integration/differentiation. Extensive studies were carried out to devise suitable techniques for data processing [46] and suitable excitation signals selection [47].

More recently there has been an extensive use of heuristic methods belonging to the family of genetic algorithms for global optimization problems. The Particle Swarm Optimization (PSO) is a gradient-free method proposed by Kennedy and Eberhart [22]. The main advantages are (i) the applicability to a single type of data without requiring differentiation or integration, (ii) the robustness against instrumental noise, and (iii) the property of converging to the global minimum of an objective function without restrictions. On the other hand, the main disadvantage consists in the lack of well-posed proofs of convergence. The PSO algorithm has been used for a wide number of applications such as topology and shape optimization [14, 15], truss and frame structures optimization [12, 19, 33], aircraft wings optimization [41]. Several variants of the original PSO algorithm have been proposed mainly targeted to the identification or optimization of nonlinear hysteretic and chaotic systems [23, 25, 48]. Charalampakis and Dimou [8] employed two variants of the PSO algorithm to calibrate the BW model parameters which best fitted the hysteretic force-displacement curves of a steel welded-bolted joint. Quaranta et al. [31] compared different PSO versions for identifying the parameters of the van der Pol-Duffing oscillators.

In this paper, a continuum hysteretic beam formulation based on the BW model of hysteresis is proposed to describe the hysteretic behavior of steel wire ropes subject to flexural cycles (see Fig. 1). The considered theory is the Special Cosserat theory of shear deformable planar beams undergoing finite displacements and rotations. A BW-type hysteretic relationship is established between the bending moment and the associated curvature. Experimental quasistatic tests are performed on assemblies of steel wire ropes, clamped at both ends, fixing one end and prescribing to the other end a cyclic displacement in the direction orthogonal to the ropes length. The restoring forces developed by the wire ropes are measured for several displacement amplitudes. The wire ropes undergo a deflection with opposite curvatures having the nodal point at the midspan. The parameters which best fit the experimentally obtained force-displacement curves are identified by means of the PSO algorithm. The proposed model represents a step forward from phenomenological towards mechanical modeling. The equivalent beam model presents the actual geometric features (length and circular cross section) and boundary conditions of the wire rope while the BW-type moment-curvature constitutive law is adopted for modeling the memory effects due to the interwire friction. Hysteresis is introduced in the bending moment according

(a)

(b)

(c)

(d)
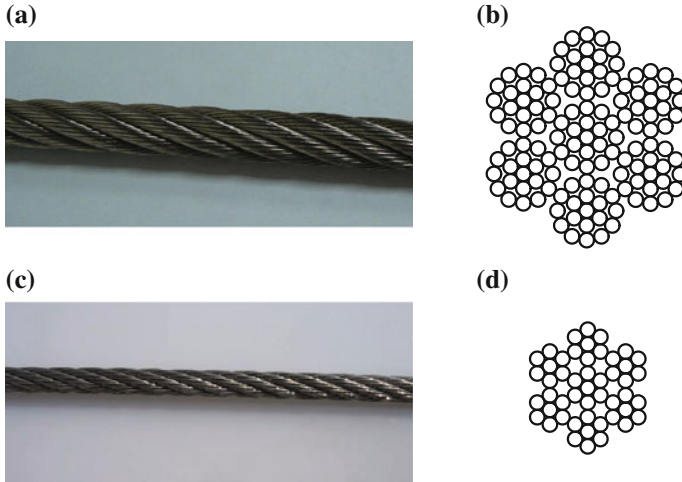
Fig. 1 The investigated wire ropes: **a** 7×19 and **c** 7×7 and their cross sections (**b**) and (**d**), respectively

to the assumption that this loading state causes most of the relative sliding of the wires. For more general loading states, hysteresis can be also associated to the axial force by defining a suitable interaction law with the hysteretic bending moment.

2 The Bouc-Wen Model of Hysteresis

The restoring force f of the BW model enhanced with a cubic term is the summation of the elastic force $k_e x + k_3 x^3$ and hysteretic force z, respectively, in which x denotes the displacement, k_e indicates the elastic stiffness and k_3 is the coefficient of the cubic restoring term. The hysteretic force evolution is described by the first-order differential equation

$$\dot{z} = [k_d - (\gamma + \beta \, \text{sgn}(z\dot{x})) \, |z|^n] \dot{x} \tag{1}$$

where k_d, γ, β and n together with k_e and k_3 are the constitutive parameters of the model and the overdot indicates differentiation with respect to time t. The tangent stiffness of the hysteretic force denoted by z_x is obtained by multiplying the left- and right-hand sides of (1) by dt, and dividing the resulting equation by dx thus giving

$$z_x = k_d - (\gamma + \beta \, \text{sgn}(z\dot{x})) \, |z|^n . \tag{2}$$

The hysteretic tangent stiffness at the origin is k_d, while the tangent stiffness of the overall restoring force f is $k_e + k_d$. Along the loading and unloading branches, the

hysteretic force z reaches upper and lower bounds equal to $\pm[k_d/(\gamma + \beta)]^{\frac{1}{n}}$ when the displacement is such that $z_x = 0$. Thus, if the cubic restoring term is set to zero, the tangent stiffness of the restoring force becomes k_e which thus represents the post-elastic stiffness. These considerations are valid only when $\gamma + \beta > 0$ for which the model exhibits a softening behavior. Moreover, these model properties can guide the initial choice of the parameters design space.

The nondimensional form of the restoring force and the evolution equation of the hysteretic component read

$$\tilde{f} = \delta\tilde{x} + (1 - \delta)\tilde{z} + \tilde{k}_3\tilde{x}^3, \tag{3}$$

$$\dot{\tilde{z}} = [1 - (\tilde{\gamma} + \tilde{\beta}\,\mathrm{sgn}(\tilde{z}\dot{\tilde{x}}))\,|\tilde{z}|^n]\dot{\tilde{x}}, \tag{4}$$

respectively, where the overdot denotes differentiation with respect to nondimensional time $\tilde{t}$ and the following nondimensional variables and parameters are introduced:

$$\tilde{x} = \frac{x}{x_0}, \qquad \tilde{t} = \omega t, \qquad \tilde{z} = \frac{z}{z_0}, \qquad \delta = \frac{k_e}{k_e + k_d}, \qquad \tilde{k}_3 = \frac{k_3 x_0^2}{k_e + k_d}. \tag{5}$$

In (5), x_0 indicates a characteristic displacement, $z_0 = k_d x_0$, $\omega = \sqrt{N_0/(x_0 m)}$ with $N_0 = (k_e + k_d)x_0$ and m denoting a characteristic mass. The other dimensionless parameters are $(\tilde{\gamma}, \tilde{\beta}) = (\gamma, \beta)x_0 z_0^{n-1}$.

3 The Hysteretic Beam Model

The formulation of the shearable nonlinear beam follows [24]. Let us consider a fixed reference frame $(O, \boldsymbol{e}_1, \boldsymbol{e}_2, \boldsymbol{e}_3)$ and a straight reference configuration for the beam centerline described by the vector $\boldsymbol{r}^o(s) = s\boldsymbol{e}_1$ where $s \in [0, l]$ is the arclength parameter and l denotes the initial beam length. The orientation of the beam cross section in the reference configuration is described by the intrinsic frame $(\boldsymbol{b}_1^o, \boldsymbol{b}_2^o, \boldsymbol{b}_3^o)$ of which $\boldsymbol{b}_1^o$ and $(\boldsymbol{b}_2^o, \boldsymbol{b}_3^o)$ are collinear with $\boldsymbol{e}_1$ and the principal axes of inertia of the cross section, respectively. The reference position of the material points of the beam is defined by the position vector $\boldsymbol{p}^o(s) = \boldsymbol{r}^o(s) + x_2(s)\boldsymbol{b}_2^o + x_3(s)\boldsymbol{b}_3^o$. The cross sections are assumed to be locally rigid implying the preservation of planarity. We consider only planar motions for the beam centerline which can be described by the displacement vector $\boldsymbol{u}(s, t) = u(s, t)\boldsymbol{e}_1 + v(s, t)\boldsymbol{e}_2$ while we let the rotation of the cross sections about $\boldsymbol{e}_3$ be described by $\theta(s, t)$. The actual configuration of the

centerline is given by the position vector $r(s, t) = r^o(s, t) + u(s, t)$ while the actual orientation of the cross sections is described by the triad (b_1, b_2, b_3). The unit vector b_1 makes the angle $\theta(s, t)$ with $b_1^o = e_1$. The position vector of a material point in the actual beam configuration is described by $p(s, t) = r(s, t) + x_2(s)b_2 + x_3(s)b_3$ where $b_1 = \cos\theta e_1 + \sin\theta e_2, b_2 = -\sin\theta e_1 + \cos\theta e_2$, and $b_3 = e_3$. The kinematic unknowns are $(u(s, t), v(s, t), \theta(s, t))$. Denoting by ∂_s differentiation with respect to s, the stretch vector is defined as $\nu := \partial_s r$ and expressed as

$$\nu(s, t) = \nu(s, t)b_1(s, t) + \eta(s, t)b_2(s, t) \tag{6}$$

where ν and η represent the beam stretch and shear strain, respectively. The third generalized strain is the bending curvature μ given by

$$\mu(s, t) = \partial_s\theta. \tag{7}$$

The stretch and the shear strain can be expressed in terms of the displacement gradient and the flexural rotation angle as

$$\nu(s, t) = (1 + \partial_s u)\cos\theta + \partial_s v\sin\theta, \qquad \eta(s, t) = -(1 + \partial_s u)\sin\theta + \partial_s v\cos\theta. \tag{8}$$

The generalized strains (ν, η, μ) are related through the constitutive relationships to the generalized stress resultants and moment resultant, also referred to as contact forces and contact couple. The contact force vector is $n = N(s, t)b_1(s, t) + Q(s, t)b_2(s, t)$ while the bending moment is $M(s, t)$. The linear constitutive equations for an elastic isotropic beam read

$$N(s, t) = EA(\nu(s, t) - 1), \qquad Q(s, t) = GA^*\eta(s, t), \qquad M(s, t) = EJ\mu(s, t), \tag{9}$$

where E and G represent Young's modulus and the shear modulus, respectively; A is the area of the cross section, A^* is the shear area and J is the area moment of inertia about the principal axis b_3.

The equations of motion read

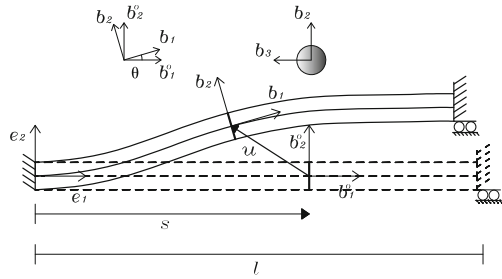$$\rho A\partial_{tt}u = (\partial_s N - \mu Q)\cos\theta - (\partial_s Q + \mu N)\sin\theta + f_1, \tag{10}$$

$$\rho A\partial_{tt}v = (\partial_s N - \mu Q)\sin\theta + (\partial_s Q + \mu N)\cos\theta + f_2, \tag{11}$$

$$\rho J\partial_{tt}\theta = \partial_s M + \nu Q - \eta N + c, \tag{12}$$

where ρ is the mass density, f_1, f_2, and c indicate the forces and the couple per unit reference length, respectively. Equations (10)–(12) are obtained from the balance of linear and angular momentum in the fixed reference frame. They are supplemented by general boundary and initial conditions expressed as

Fig. 2 The planar beam in the reference (*dashed lines*) and actual configurations (*solid lines*)

$$\boldsymbol{u}(0, t) = \overline{\boldsymbol{u}}(t), \quad \theta(0, t) = \overline{\theta}(t), \qquad \boldsymbol{u}(l, t) = \widehat{\boldsymbol{u}}(t), \quad \theta(l, t) = \widehat{\theta}(t) \qquad t \in [0, T], \tag{13}$$

$$\boldsymbol{u}(s, 0) = \check{\boldsymbol{u}}(s), \quad \theta(s, 0) = \check{\theta}(s) \qquad s \in [0, l], \tag{14}$$

where $[0, T]$ denotes the time integration domain. Figure 2 shows the beam in the reference configuration that undergoes a planar motion to the actual configuration.

In the present model, hysteresis is introduced in the constitutive equation $(9)_3$ between the bending moment and the flexural curvature. The hysteretic constitutive equation reads

$$M(s, t) = EJ_e \mu + M_h + k_3 \mu^3 \tag{15}$$

where k_3 represents the coefficient of the cubic elastic bending moment, M_h is the hysteretic bending moment whose evolution is governed by the first-order differential equation

$$\partial_t M_h = \left\{ EJ_h - \left[\gamma + \beta \, \text{sgn}(M_h \partial_t \mu) \right] |M_h|^n \right\} \partial_t \mu \tag{16}$$

with ∂_t denoting differentiation with respect to time t. The parameters (γ, β, n) are the same as those defined in (1). The tangent stiffness of the bending moment at the origin $\mu = 0$ is $EJ_t = EJ_e + EJ_h$ while the post-elastic bending stiffness is EJ_e, attained when $\partial_t M_h = 0$, $M_h = \pm [EJ_h/(\gamma + \beta)]^{\frac{1}{n}}$ and $k_3 = 0$.

The main objective of the hysteretic beam model is to describe the experimentally obtained hysteretic responses of steel wire ropes subject to bending cycles. The nonlinear beam model can reproduce the actual geometry (length and cross section) of the wire rope, boundary and loading conditions during the tests. The hysteretic bending moment, introduced in the constitutive equation, has the designated function of describing the hysteretic behavior due to the interwire friction within the rope. The beam cross section is assumed as the circular envelope of the actual cross section of the wire rope. However, to take into account the fact that the cross section of a wire rope is not compact but is constituted by an assembly of individual wires, an additional parameter $\psi \in (0, 1]$ is introduced to reduce the bending stiffness EJ of

the compact circular cross section bounding the actual rope cross section. By letting the new parameter $\delta \in (0, 1)$ denote the post-elastic-to-elastic bending stiffness (in the limit $n = \infty$), we set

$$EJ_t = \psi EJ, \qquad \frac{EJ_e}{EJ_t} = \delta, \qquad \frac{EJ_h}{EJ_t} = 1 - \delta. \tag{17}$$

The parts of the bending stiffness indicated by EJ_e and EJ_h, respectively, can be written as

$$EJ_e = \delta EJ_t = \delta \psi EJ, \qquad EJ_h = (1 - \delta)EJ_t = (1 - \delta)\psi EJ. \tag{18}$$

The beam length, Young's modulus, cross section (zeroth and second area moments), boundary and loading conditions are assumed on the basis of the actual wire ropes geometrical and mechanical features. The hysteresis parameters (γ, β, n) and the stiffness parameters (ψ, δ) are calibrated to best fit the experimental measurements. This model has the purpose of describing, among other goals, the applications exploiting the frictional dissipation of wire ropes [4, 5]. The hysteretic features of the response of a given wire rope type under bending can be evaluated carrying out an experimental campaign whose results are used for identifying the parameters of the proposed model. The advantage is that the identified model of a given wire rope can be used during the design process of the specific application which makes use of wire ropes thus drastically reducing the number of experimental tests required and the overall design costs.

Equations (10)–(12) can be rendered nondimensional introducing the following nondimensional variables and parameters [24]: $\tilde{s} = s/l$, $\tilde{t} = \omega_c t$, $\tilde{u} = u/l$, $\tilde{v} = v/l$, $\omega_c = [EJ/(\rho A l^4)]^{1/2}$, $k_a = EAl^2/(EJ)$, $k_s = GA^*l^2/(EJ)$, $\tilde{k}_3 = k_3/(EJ)$, $(\tilde{f}_1, \tilde{f}_2) = (f_1, f_2)l^3/(EJ)$, $\tilde{c} = cl^2/(EJ)$. The nondimensional hysteretic moment is given by

$$\tilde{M}_h = M_h l/EJ \tag{19}$$

whose evolution is described by the following nondimensional equation:

$$\partial_{\tilde{t}} \tilde{M}_h = \left\{ (1 - \delta)\psi - \left[\tilde{\gamma} + \tilde{\beta}\, \mathrm{sgn}(M_h \partial_{\tilde{t}}\mu) \right] \left| \tilde{M}_h \right|^n \right\} \partial_{\tilde{t}}\mu \tag{20}$$

where

$$\tilde{\gamma} = \gamma(EJ)^{n-1}/l^n, \qquad \tilde{\beta} = \beta(EJ)^{n-1}/l^n. \tag{21}$$

The nondimensional equations of motion read

$$\partial_{\tilde{t}\tilde{t}}\tilde{u} = [k_a \partial_{\tilde{s}}\nu - k_s \eta \partial_{\tilde{s}}\theta]\cos\theta - [k_s \partial_{\tilde{s}}\eta + k_a(\nu - 1)\partial_{\tilde{s}}\theta]\sin\theta + \tilde{f}_1, \tag{22}$$

$$\partial_{\tilde{t}\tilde{t}}\tilde{v} = [k_a \partial_{\tilde{s}}\nu - k_s \eta \partial_{\tilde{s}}\theta]\sin\theta + [k_s \partial_{\tilde{s}}\eta + k_a(\nu - 1)\partial_{\tilde{s}}\theta]\cos\theta + \tilde{f}_2, \tag{23}$$

$$\partial_{\tilde{t}\tilde{t}}\theta/k_a = (\psi\delta + \tilde{k}_3)\partial_{\tilde{s}\tilde{s}}\theta + \partial_{\tilde{s}}\tilde{M}_h + k_s\nu\eta - k_a(\nu-1)\eta + \tilde{c} \qquad (24)$$

where the assumption that the beam has a uniform cross section along the overall span has been adopted. These equations are supplemented by boundary and initial conditions expressed by (13) and (14). The solution can be obtained via a finite element discretization [24]. The solution at each step is obtained employing a Newton-Raphson iterative scheme.

4 Experimental Bending Tests for Steel Wire Ropes

The complex geometry of the contact areas between the wires of spiral and stranded wire ropes makes the experimental tests necessary for quantifying the dissipation capacity. An experimental campaign was carried out to evaluate the hysteresis cycles of two stranded steel wire ropes subject to bending cycles. The investigated wire ropes have a diameter equal to 10 and 6 mm and are constituted by 7 strands of 19 steel wires and 7 strands of 7 steel wires of diameter equal to 0.65 mm, respectively. Figure 1 shows the wire ropes and their cross sections. The tests were performed employing the Material Testing System (MTS) in the DISG laboratory at Sapienza University of Rome (Italy). Two groups of four parallel 7×19 and 7×7 wire ropes were tested with the experimental setup illustrated in Fig. 3. The wire ropes ends are clamped at the two thick steel bars denoted by B_1 and B_2, the former being connected to the piston P of the MTS machine. Bar B_2 is passed through by two smooth rods (denoted by S_1 and S_2) and one threaded cylindrical rod (denoted by t). The threaded bar does not touch the bar B_2 while between the smooth rods s_1 and s_2 and B_2 two self-lubricated clinched joints are placed to allow a relative frictionless sliding. The rods t, s_1 and s_2 are welded to a third steel bar denoted by B_3 that is, in turn, fixed to a load cell.

A sinusoidal displacement with a relatively low frequency equal to 0.1 Hz is applied to B_1 along the direction orthogonal to the wire ropes whose restoring force is measured by the load cell (see Fig. 3). The wire ropes are subject to pure bending thanks to the free sliding of bar B_2 on rods s_1 and s_2. The two bolts (denoted by b_1 and b_2) on the threaded bar t can be used both for mounting the system and realizing another testing setup in which the sliding of B_2 is prevented. In the latter case, tensile loads arise in the ropes and the measured force-displacement curves exhibit a strong hardening behavior. In this paper only pure bending tests are presented.

Figure 4 shows the experimental setup with the undeformed and some deformed configurations of the specimen. The wire ropes present a deflected shape characterized by a change of curvature through the midspan. Table 1 lists the experimental tests for the 7×19 and 7×7 wire ropes. For each wire rope length and displacement amplitude, 15 hysteresis cycles were measured to obtain a stabilized loop.

Fig. 3 Experimental setup
with the tested wire ropes
and their fixtures. The *arrow*
indicates the cyclic
displacement provided by
the MTS testing machine
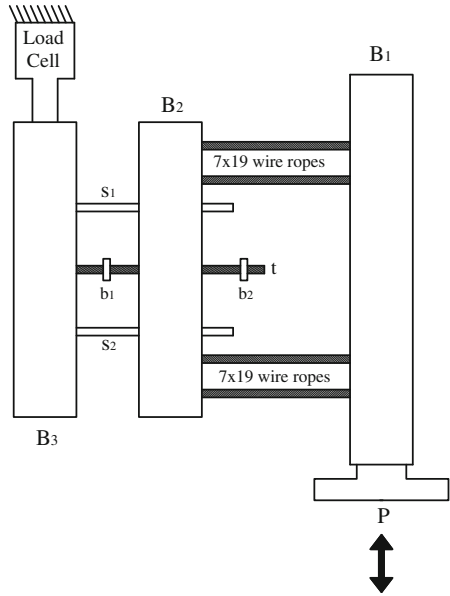
Fig. 4 The experimental
setup showing the wire ropes
in the undeformed (**a**) and
deformed (**b**), (**c**)
configurations
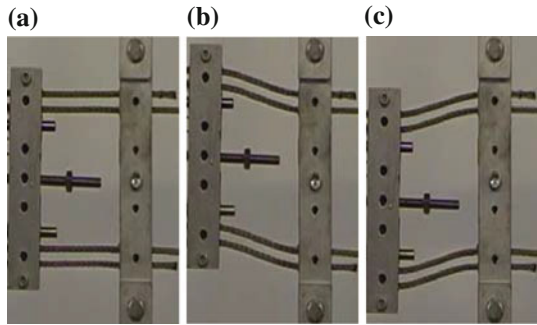
Table 1 List of the performed experimental tests in which the wire rope section, the wire rope length and the prescribed displacement are indicated

Wire rope cross section	Length (mm)	Displacement amplitude (mm)			
7×19	75	5	10	15	20
7×19	85	5	10	15	20
7×19	90	5	10	15	–
7×7	100	5	10	15	20

5 Particle Swarm Optimization Algorithm

Particle Swarm Optimization (PSO) is a heuristic global optimization method based on the swarm intelligence theory and inspired from the social interactions in bird flocks, schools of fish or swarms of insects. The algorithm starts from an initial population (the particles) formed by several sets of parameters to optimize with respect to an objective function (OF). Each particle is modified iteratively by a velocity vector that is function of the best particle within the population and the best values assumed by the particle itself until the considered iteration.

Here, we seek to identify the model parameters of the hysteretic beam which best fit the experimentally obtained restoring forces as function of the prescribed displacements. The measured restoring force is denoted by $f(y)$ while the model-based restoring force is indicated by $\hat{f}(y)$. The mean square error (MSE) between measured and model-based restoring forces is assumed as objective function to minimize and expressed as

$$OF(\boldsymbol{x}) = \frac{\sum_{k=1}^{N} [f(y_k) - \hat{f}(y_k|\boldsymbol{x})]^2}{N\sigma_f^2} \tag{25}$$

where σ_f^2 and N are the variance and the number of samples of the experimentally obtained restoring force, respectively, $\boldsymbol{x}$ denotes the parameters vector of the model, and y indicates the displacement. Considering the particles $\boldsymbol{x}_i$ ($i = 1, 2, .., p$) and the lower and upper bounds $\boldsymbol{x}_{LB}$ and $\boldsymbol{x}_{UB}$ for the particle values, respectively, the initial population is a matrix formed by p vectors whose values are drawn by a Gaussian distribution on their ranges of variation. The particles are updated at the jth iteration according to the following expression:

$$\boldsymbol{x}_{i,j+1}^k = \boldsymbol{x}_{i,j} + \boldsymbol{v}_{i,j+1}^k \qquad i = 1, 2, .., p, \quad j = 1, 2, .., q \tag{26}$$

where time is assumed to be equal to unity and q is the number of iterations. The velocity is

$$\boldsymbol{v}_{i,j+1} = w\boldsymbol{v}_{i,j} + c_1\boldsymbol{r}_1 \circ (\boldsymbol{p}_{i,j} - \boldsymbol{x}_{i,j}) + c_2\boldsymbol{r}_2 \circ (\boldsymbol{p}_j - \boldsymbol{x}_{i,j}) \tag{27}$$

where w is the inertia factor; c_1, c_2 are the cognitive and social parameters, respectively. These parameters in the simple PSO algorithm are constant and can be set to $w = 0.8$, $c_1 = 2.8$, and $c_2 = 1.3$. A study about the effect of the values assigned at the inertia factor and cognitive and social parameters can be found in [13]. The vector $\boldsymbol{p}_{i,j}$ represents the ith best ever particle at the jth iteration with respect to the criterion expressed by (25). The vector $\boldsymbol{p}_j$ denotes the best ever particle at the jth iteration between all vectors of the population. The notation $\circ$ indicates element-by-element multiplication and the vectors $\boldsymbol{r}_1$ and $\boldsymbol{r}_2$ are formed by random variables

with uniform distributions in the interval [0, 1]. When a particle element exceeds the assigned range of variation, its value is reset to the value belonging to the closest boundary. The number of iterations q is chosen by the user according to the values achieved by MSE that must be lower than a given tolerance for which the identification is considered acceptable.

6 Identification Results

The experimentally obtained force-displacement hysteresis cycles are identified using the proposed hysteretic beam model. The measured restoring forces are divided by the number of wire ropes according to the fact that they work in parallel and equally contribute to the total restoring force. The tests with the 7×19 wire rope of length equal to 75 mm are identified with an individual parameters set for each displacement amplitude. The set of model parameters, obtained by averaging the thus obtained values, is used to compute the hysteresis cycles for the other wire ropes lengths and compared with the experimental measurements. The test with the 7×7 wire rope for a displacement amplitude equal to 15 mm is identified with a parameters set that is later employed to compute the hysteresis cycles for different displacement amplitudes. Thus, the model-based cycles are compared with the experimentally obtained curves.

The same geometric features and boundary conditions of the wire ropes are assigned to the hysteretic beam. In particular, the beam length and the diameter of the circular cross section are assumed equal to those of the wire ropes. The beam ends are both clamped. The Young modulus and Poisson coefficient are assumed equal to 206 GPa and 0.3, respectively, while the parameters $(\psi, \delta, \gamma, \beta, n, k_3)$ to identify are assigned ranges of variation according to the PSO algorithm. One end of the beam (i.e., that at $s = l$) is subject to the displacement $x = A \sin \omega t$ along e_2 (see Fig. 2) where A is the amplitude (equal, in turn, to that of the experimental tests), $\omega = 0.628$ rad/s is the circular frequency, and $t \in (0, T)$ is the time. The generalized force $f(s, t) = N(s, t) \sin \theta(s, t) + Q(s, t) \cos \theta(s, t)$ along e_2 at $s = 0$, which coincides with the shear force $Q(0, t)$ (since the clamp implies $\theta(0, t) = 0$), is the restoring force. Therefore, $(x(t), f(0, t), t \in (t_1, t_2))$ represent the displacement and force to compare with the experimental measurements, t_1 and t_2 are the time instants delimiting a stabilized hysteresis cycle. Time t can be seen as a parameter because the frequency ω is assumed so low that the inertia forces and rotary inertia become negligible. The boundary and initial conditions for the beam can be summarized as follows

$$u(0, t) = \theta(0, t) = 0, \qquad v(l, t) = x(t), \quad \theta(l, t) = 0, \qquad t \in [0, T] \qquad (28)$$

$$u(s, 0) = \theta(s, 0) = 0, \qquad s \in [0, l]. \qquad (29)$$

Note that the horizontal displacement $u(t)$ at $s = l$ is not restricted.

The identification task is performed employing concurrently the finite element solver COMSOL Multiphysics [29] and Matlab [42]. The computational architecture is managed by Matlab to which the input data are fed. COMSOL Multiphysics is used for the computation of the hysteretic beam response across the beam span. At each iteration of the PSO algorithm, the beam model parameters, evaluated by Matlab, are given as input to COMSOL that performs the finite element discretization and solves the problem. The vectors (x, f) are fed back to Matlab for computing the OF (i.e., MSE) and performing the identification. The number of particles p and iterations q are set to 10 and 75, respectively. Table 2 shows the assigned ranges of variation for the parameters to identify. The coefficient of the cubic term k_3 is set to zero a priori and is not reported in the following results. These initial input data are evaluated by means of some preliminary calculations.

Table 3 summarizes the optimal parameter sets selected by the PSO algorithm for the 7×19 wire rope whose length is 75 mm while in Fig. 5 the comparisons between the model-based and the experimentally obtained hysteresis cycles are shown. The identification is accurately performed and the parameters which exhibit the lowest variation with the displacement amplitude are ψ and δ regulating the elastic and hysteretic stiffnesses. This suggests that the hysteretic beam model is suitable for reproducing the hysteretic wire ropes response. For the displacement amplitude of 20 mm (Fig. 5d), both the experimentally obtained and model-based restoring forces show a slight hardening. This is more pronounced for the model-based curves and is due to the geometric effect of the bending curvature that takes finite values. Figure 6 shows a cycle of (a) the total and (b) the hysteretic bending moments as function of the curvature at $s = 0$ for the beam length equal to 75 mm and the prescribed end

**Table 2** Ranges of variation for the parameters to identify

	ψ (–)	δ (–)	γ ($N^{1-n}m^{2-n}$)	β ($N^{1-n}m^{2-n}$)	n (–)
Min	0.008	0.1	0.8	0.8	1.0
Max	0.025	0.6	2	2	1.3

Table 3 Identified parameters and associated MSEs for the 7×19 wire rope of length equal to 75 mm

A (mm)	ψ (–)	δ (–)	γ ($N^{1-n}m^{2-n}$)	β ($N^{1-n}m^{2-n}$)	n (–)	MSE (%)
5	0.0159	0.251	1.478	1.729	1.275	0.43
10	0.0162	0.240	1.391	1.103	1.152	0.44
15	0.0166	0.21	1.218	1.151	1.165	0.40
20	0.0168	0.186	1.684	1.989	1.285	0.50
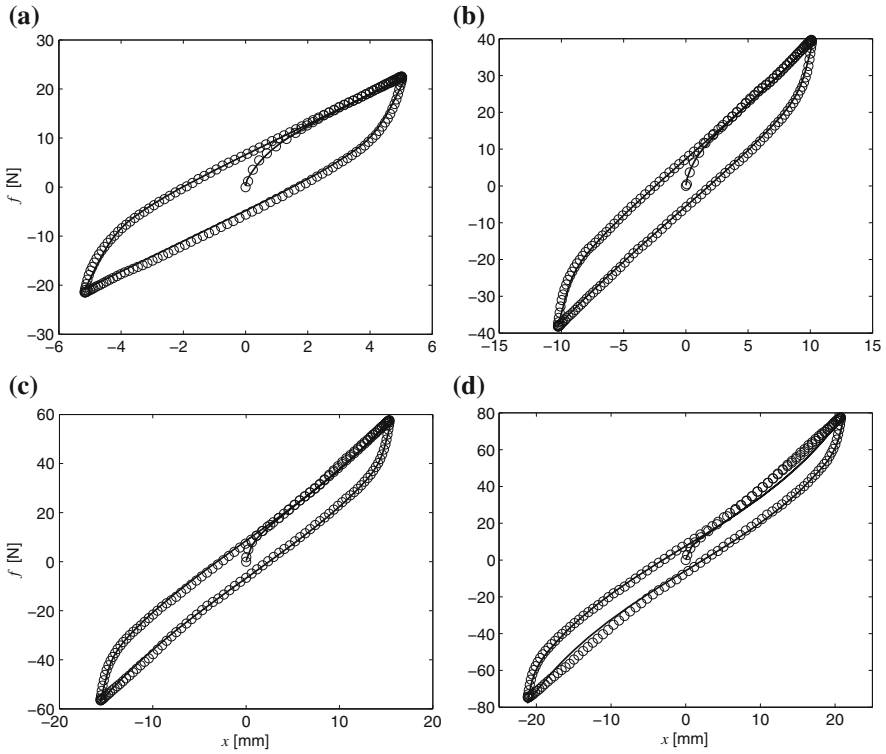
Fig. 5 Comparison between the experimentally obtained (*circles*) and model-based (*solid lines*) hysteresis cycles for displacement amplitudes equal to 5 mm (**a**), 10 mm (**b**), 15 mm (**c**) and 20 mm (**d**); the employed model parameters are reported in Table 3 and the identified tests are those for the 7×19 wire rope of length equal to 75 mm
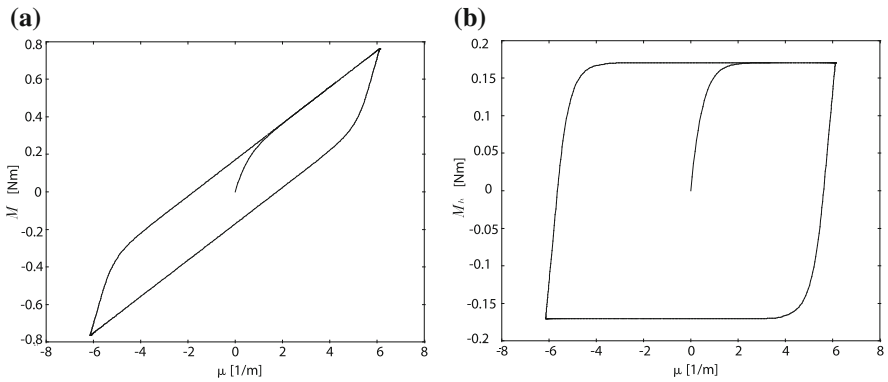

Fig. 6 a Total and **b** hysteretic bending moments versus the curvature at $s = 0$ for the beam length of 75 mm with the model parameters of Table 4 and the prescribed end displacement equal to 5 mm

(a)

(b)
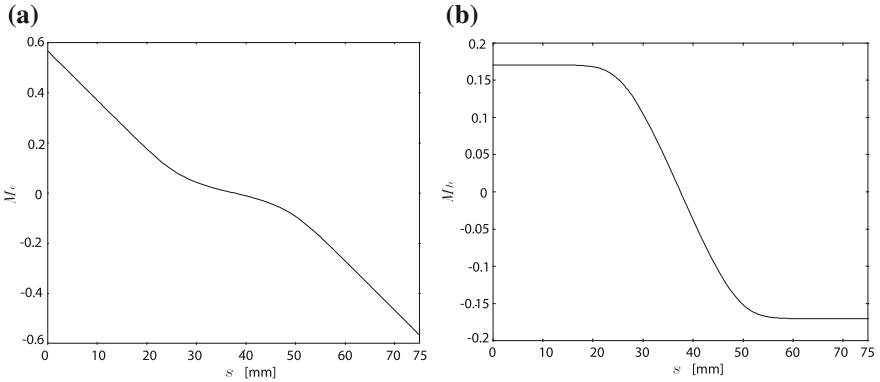
Fig. 7 **a** Elastic and **b** hysteretic bending moments across the beam span whose length is equal to 75 mm with the model parameters of Table 4 and for the prescribed end displacement equal to 5 mm

Table 4 Values of the model parameters obtained as mean values of the parameters in Table 3

ψ (–)	δ (–)	γ (N^{1-n}m^{2-n})	β (N^{1-n}m^{2-n})	n (–)
0.0164	0.222	1.443	1.493	1.219

(a)

(b)
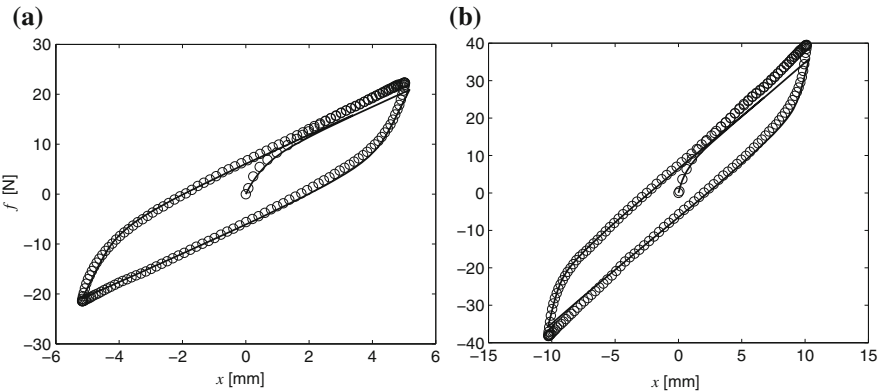
Fig. 8 Comparison between the experimentally obtained (*circles*) and model-based (*solid lines*) hysteresis cycles for displacement amplitudes equal to 5 mm (**a**) and 10 mm (**b**); the employed model parameters are reported in Table 3 and the identified tests are those for the 7×19 wire rope whose length is 75 mm

displacement of 5 mm. The elastic and hysteretic bending moments along the beam length are illustrated in Fig. 7. The mean values of the model parameters reported in Table 4 are used to reproduce the hysteresis curves for the other wire rope lengths. Figures 8, 9 and 10 show the comparisons between the model-based and the experimentally obtained hysteresis cycles for the wire rope lengths of 75, 80, and 90 mm, respectively. The associated MSEs are given in Table 5. The mean values of the
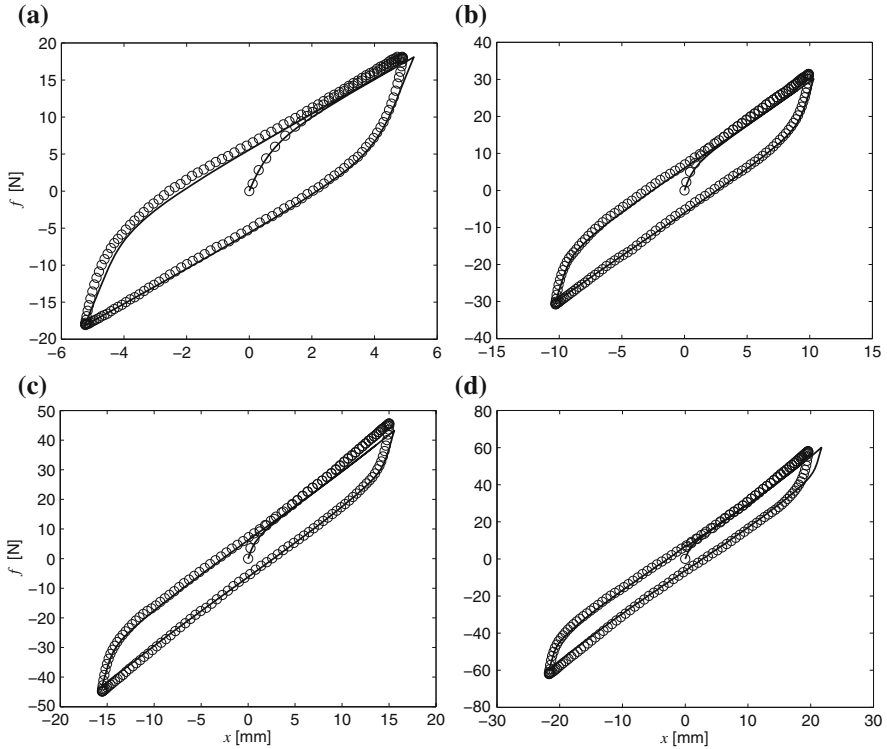
Fig. 9 Comparison between the experimentally obtained (*circles*) and model-based (*solid lines*) hysteresis cycles for displacement amplitudes equal to 5 mm (**a**), 10 mm (**b**), 15 mm (**c**) and 20 mm (**d**); the employed model parameters are reported in Table 4 and the identified tests are those for the 7×19 wire rope whose length is 80 mm

parameters identified for the 7×19 wire rope of length equal to 75 mm are capable of accurately describing the hysteresis curves obtained for the lengths equal to 75, 80, and 90 mm. The best results are achieved for the displacement amplitudes of 5, 10 and 15 mm while for the displacement amplitude of 20 mm some discrepancies are observed. This loss of accuracy is mainly due to the hardening behavior exhibited by both the model-based and experimentally obtained hysteretic cycles for large displacement amplitudes. The hardening is more significant in the model-based response, thus a variation of the constitutive parameters for different displacement amplitudes is required for an accurate description of the experimentally obtained curves. However, the achieved accuracy level is consistent with the practical requirements.
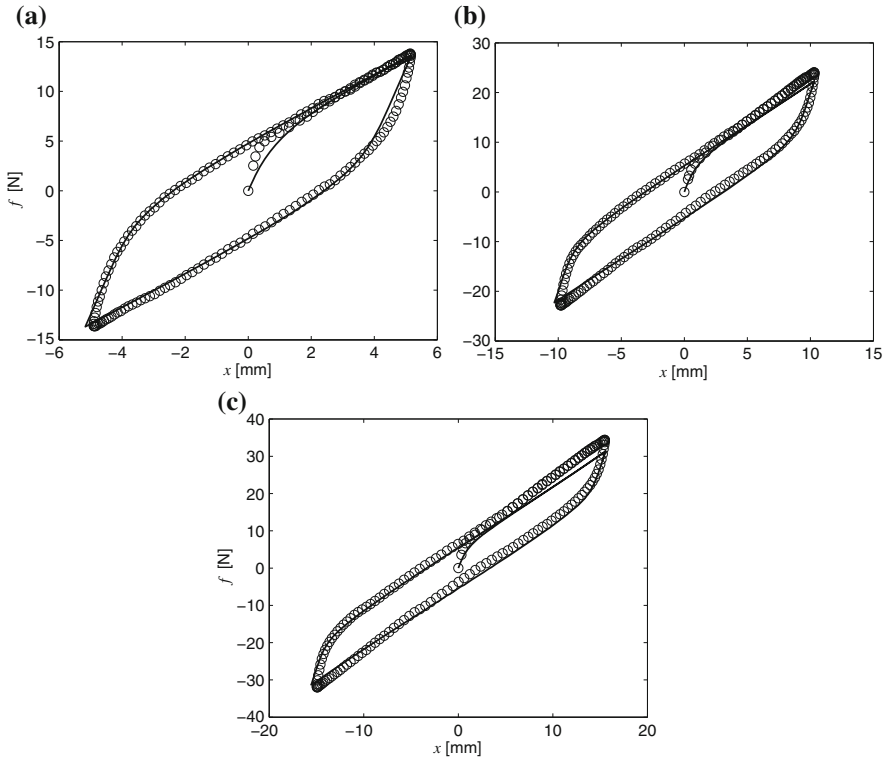
Fig. 10 Comparison between the experimentally obtained (*circles*) and model-based (*solid lines*) hysteresis cycles for displacement amplitudes equal to 5 mm (**a**), 10 mm (**b**) and 15 mm (**c**); the employed model parameters are reported in Table 4 and the identified tests are those for the 7×19 wire rope whose length is 90 mm

The experimentally obtained hysteretic cycles for the 7×7 wire rope can be accurately described identifying the model parameters according to a single displacement amplitude cycle. This is due to the fact that the ratio between the displacement amplitudes and wire rope length is small enough to induce weak nonlinearities and the parameters change with the displacement amplitude is negligible. In Table 6 the parameters identified for fitting the hysteretic curve of the 7×7 wire rope for a displacement amplitude equal to 15 mm are shown. The comparisons between the experimentally obtained and model-based curves are shown in Fig. 11 with the associated MSEs given in Table 7.
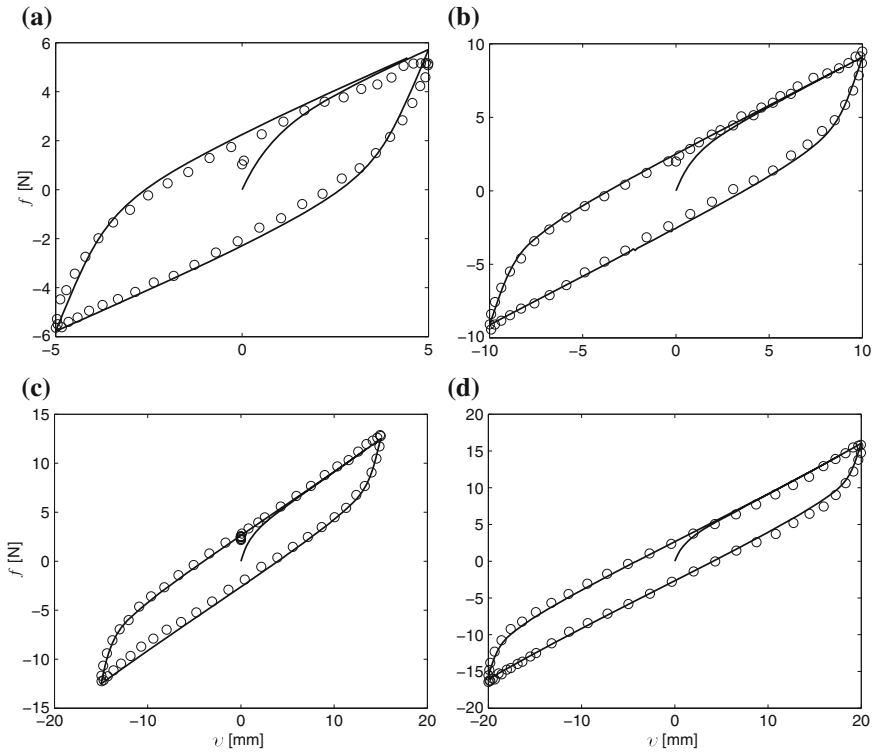
Fig. 11 Comparison between the experimentally obtained (*circles*) and model-based (*solid lines*) hysteresis cycles for displacement amplitudes equal to 5 mm (**a**), 10 mm (**b**), 15 mm (**c**) and 20 mm (**d**); the employed model parameters are reported in Table 6 and the identified tests are those for the 7×7 wire rope

Table 5 MSEs between the model-based and experimentally obtained hysteresis cycles of Figs. 8, 9 and 10, identified by the wire rope type, length l and displacement amplitude A

Wire rope type	l (mm)	A (mm)	MSE (%)
7×19	75	5	0.63
7×19	75	10	0.92
7×19	80	5	0.94
7×19	80	10	0.89
7×19	80	15	0.53
7×19	80	20	0.68
7×19	90	5	0.71
7×19	90	10	0.71
7×19	90	15	0.87

Table 6 Identified model parameters which best fit the experimentally obtained hysteretic curve of the 7×7 wire rope for a displacement amplitude equal to 15 mm

ψ (–)	δ (–)	γ (N^{1-n}m^{2-n})	β (N^{1-n}m^{2-n})	n (–)
0.0355	0.201	1.987	1.188	1.134

Table 7 MSEs between the model-based and experimentally obtained hysteresis cycles of Fig. 11, identified according to the wire rope type, length l and displacement amplitude A

Wire rope type	l (mm)	A (mm)	MSE (%)
7×7	100	5	1.1
7×7	100	10	0.68
7×7	100	15	0.45
7×7	100	20	0.51

7 Conclusions

A nonlinear hysteretic beam model based on the formulation of an equivalent shear deformable beam with geometric nonlinearities and an extension of the Bouc-Wen model of hysteresis to the one-dimensional polar continuum was proposed. Hysteresis is introduced in the constitutive equation for the bending moment given as a direct summation of elastic and hysteretic components. The model aims to describe the hysteretic behavior of steel wire ropes subject to bending cycles. Experimental tests were performed by means of an *ad hoc* setup for evaluating the restoring force exhibited by a group of steel wire ropes clamped at both ends and subject to a quasistatic displacement of one end in the direction orthogonal to the wire ropes rest position. The energy dissipation within the wire ropes is due to the interwire friction. Several tests were executed for three lengths of the wire ropes and for different prescribed displacement amplitudes. The proposed model reduces the actual wire rope to a compact nonlinear beam in which the hysteretic bending moment describes the frictional dissipation in a phenomenological fashion and the Cosserat-type nonlinear beam formulation reproduces the actual mechanics. Thus the geometric and boundary conditions of the beam are assumed as those of the wire ropes while the dissipation properties are identified on the basis of experimental tests. Moreover, the bending stiffness is reduced by an additional parameter denoted by ψ to take into account the lack of compactness of the rope with respect to the equivalent cylindrical rod. The parameters regulating the hysteretic moment and the parameter ψ were identified using the PSO algorithm by best fitting the experimentally obtained curves for the 7×19 wire rope of length equal to 75 mm and for the 7×7 wire rope subject to a displacement amplitude of 15 mm. Thus, the identified parameters were employed to reproduce the hysteresis curves obtained for different lengths of the 7×19 wire rope and for different displacement amplitudes of the 7×7 wire rope. These curves show a good agreement with the experimental results confirming that the proposed

model is a valid tool for the design of a wide range of applications based on wire ropes hysteretic behaviors.

References

1. Baber, T., Noori, M.: Random vibration of degrading, pinching systems. J. Eng. Mech. **111**(8), 1010–1026 (1985)
2. Baber, T., Wen, Y.: Random vibration hysteretic, degrading systems. J. Eng. Mech. Div. **107**(6), 1069–1087 (1981)
3. Bouc, R.: Forced vibration of mechanical systems with hysteresis. In: Proceedings of the Fourth Conference on Non-linear oscillation, Prague, Czechoslovakia (1967)
4. Carboni, B., Lacarbonara, W.: A new vibration absorber based on the hysteresis of multi-configuration nitinol-steel wire ropes assemblies. In: MATEC Web of Conferences, vol. 16, p. 01004. EDP Sciences (2014)
5. Carboni, B., Lacarbonara, W., Auricchio, F.: Hysteresis of multiconfiguration assemblies of nitinol and steel strands: experiments and phenomenological identification. J. Eng. Mech. **141**, 04014135 (2014)
6. Carpineto, N., Lacarbonara, W., Vestroni, F.: Hysteretic tuned mass dampers for structural vibration mitigation. J. Sound Vib. **333**(5), 1302–1318 (2014)
7. Casciati, F.: Stochastic dynamics of hysteretic media. Struct. Saf. **6**(2), 259–269 (1989)
8. Charalampakis, A., Dimou, C.: Identification of bouc-wen hysteretic systems using particle swarm optimization. Comput. Struct. **88**(21), 1197–1205 (2010)
9. Costello, G.: Theory of Wire Rope. Springer, New York (1990)
10. Crawley, E.F., ODonnell, K.J.: Identification of nonlinear system parameters in joints using the force-state mapping technique. AIAA Pap **86**(1013), 659–667 (1986)
11. Demetriades, G., Constantinou, M., Reinhorn, A.: Study of wire rope systems for seismic protection of equipment in buildings. Eng. Struct. **15**(5), 321–334 (1993)
12. Dimou, C., Koumousis, V.: Reliability-based optimal design of truss structures using particle swarm optimization. J. Comput. Civil Eng. **23**(2), 100–109 (2009)
13. Eberhart, R.C., Shi, Y.: Particle swarm optimization: developments, applications and resources. In: Proceedings of the 2001 Congress on Evolutionary Computation, 2001, vol. 1, pp. 81–86. IEEE (2001)
14. Fourie, P., Groenwold, A.: The particle swarm optimization algorithm in size and shape optimization. Struct. Multi. Optim. **23**(4), 259–267 (2002)
15. Fourie, P., Groenwold, A.A.: Particle swarms in topology optimization. In: Proceedings of the Fourth World Congress of Structural and Multidisciplinary Optimization, Dalian, China (2001)
16. Gerges, R.: Model for the force-displacement relationship of wire rope springs. J. Aerosp. Eng. **21**(1), 1–9 (2008)
17. Gerges, R., Vickery, B.: Parametric experimental study of wire rope spring tuned mass dampers. J. Wind Engi. Ind. Aerodyn. **91**(12), 1363–1385 (2003)
18. Gerges, R., Vickery, B.: Optimum design of pendulum-type tuned mass dampers. Struct. Des. Tall Spec. Build. **14**(4), 353–368 (2005)
19. Gholizadeh, S., Salajegheh, E.: Optimal design of structures subjected to time history loading by swarm intelligence and an advanced metamodel. Comput. Methods Appl. Mech. Eng. **198**(37), 2936–2949 (2009)
20. Gnanavel, B., Gopinath, D., Parthasarathy, N.: Effect of friction on coupled contact in a twisted wire cable. J. Appl. Mech. **77**(2), 024501 (2010)

21. Gnanavel, B., Parthasarathy, N.: Effect of interfacial contact forces in radial contact wire strand. Arch. Appl. Mech. **81**(3), 303–317 (2011)
22. Kennedy, J., Eberhart, R.: Particle swarm optimization. In: Proceedings of IEEE International Conference of Neural Network IV, Perth, Australia
23. Kwok, N., Ha, Q., Nguyen, T., Li, J., Samali, B.: A novel hysteretic model for magnetorheological fluid dampers and parameter identification using particle swarm optimization. Sens. Actuators A: Phys. **132**(2), 441–451 (2006)
24. Lacarbonara, W.: Nonlinear Structural Mechanics: Theory, Dynamical Phenomena and Modeling. Springer, New York (2013)
25. Liu, B., Wang, L., Jin, Y.H., Tang, F., Huang, D.X.: Directing orbits of chaotic systems by particle swarm optimization. Chaos, Solitons Fractals **29**(2), 454–461 (2006)
26. Love, A.E.H.: A Treatise on the Mathematical Theory of Elasticity. Cambridge University Press, Cambridge (2013)
27. Ma, J., Ge, S.R., Zhang, D.K.: Distribution of wire deformation within strands of wire ropes. J. China Univ. Min. Technol. **18**(3), 475–478 (2008)
28. Masri, S., Caughey, T.: A nonparametric identification technique for nonlinear dynamic problems. J. Appl. Mech. **46**(2), 433–447 (1979)
29. Multiphysics, C.: Version 3.5 a (2008)
30. Nucera, C., di Scalea, F.L.: Monitoring load levels in multi-wire strands by nonlinear ultrasonic waves. Struct. Health Monit. **10**(6), 617–629 (2011)
31. Quaranta, G., Monti, G., Marano, G.C.: Parameters identification of van der pol-duffing oscillators via particle swarm optimization and differential evolution. Mech. Syst. Sig. Process. **24**(7), 2076–2095 (2010)
32. Sauter, D., Hagedorn, P.: On the hysteresis of wire cables in stockbridge dampers. Int. J. Nonlinear Mech. **37**(8), 1453–1459 (2002)
33. Schutte, J., Groenwold, A.: Sizing design of truss structures using particle swarms. Struct. Multi. Optim. **25**(4), 261–269 (2003)
34. Simeonov, V.K., Sivaselvan, M.V., Reinhorn, A.M.: Nonlinear analysis of structural frame systems by the state-space approach. Comput. Aided Civil Infrastruct. Eng. **15**(2), 76–89 (2000)
35. Sivaselvan, M.V., Reinhorn, A.M.: Hysteretic models for deteriorating inelastic structures. J. Eng. Mech. **126**(6), 633–640 (2000)
36. Stockbridge, G.: Vibration damper. US patent 1,675,391 (1928)
37. Tinker, M., Cutchins, M.: Damping phenomena in a wire rope vibration isolation system. J. Sound Vib. **157**(1), 7–18 (1992)
38. Triantafyllou, S., Koumousis, V.: Bouc-wen type hysteretic plane stress element. J. Eng. Mech. **138**(3), 235–246 (2011)
39. Triantafyllou, S., Koumousis, V.: Small and large displacement dynamic analysis of frame structures based on hysteretic beam elements. J. Eng. Mech. **138**(1), 36–49 (2011)
40. Triantafyllou, S.P., Koumousis, V.K.: An hysteretic quadrilateral plane stress element. Arch. Appl. Mech. **82**(10–11), 1675–1687 (2012)
41. Venter, G., Sobieszczanski-Sobieski, J.: Multidisciplinary optimization of a transport aircraft wing using particle swarm optimization. Struct. Multi. Optim. **26**(1–2), 121–131 (2004)
42. Version, M.: 7.10. 0.499 (r2010a) (2010)
43. Vestroni, F., Lacarbonara, W., Carpineto, N.: Hysteretic tuned mass damper for passive control of mechanical vibration. Sapienza University of Rome, Italian Patent No. RM2011A000434 (2011)
44. Waisman, H., Montoya, A., Betti, R., Noyan, I.: Load transfer and recovery length in parallel wires of suspension bridge cables. J. Eng. Mech. **137**(4), 227–237 (2010)
45. Wen, Y.: Method for random vibration of hysteretic systems. J. Eng. Mech. Div. **102**(2), 249–263 (1976)
46. Worden, K.: Data processing and experiment design for the restoring force surface method, part i: integration and differentiation of measured time data. Mech. Syst. Sig. Process. **4**(4), 295–319 (1990)

47. Worden, K.: Data processing and experiment design for the restoring force surface method, part ii: choice of excitation signal. Mech. Syst. Sig. Process. **4**(4), 321–344 (1990)
48. Ye, M.: Parameter identification of dynamical systems based on improved particle swarm optimization. In: Intelligent Control and Automation, pp. 351–360. Springer, Berlin (2006)